Geophysical Research Letters

RESEARCH LETTER
10.1029/2025GL119973

The Magnetic Signature of Stress in Rocks

B. R. Kugabalan[1,2], T. M. Mitchell[2], A. R. Muxworthy[1,2], W. Williams[3], H. Gregov[1], F. M. Aben[4], D. P. Dobson[2], U. D. Bellon[3], and P. G. Meredith[2]

[1]Department of Earth Science and Engineering, Imperial College London, London, UK, [2]Department of Earth Sciences, University College London, London, UK, [3]School of Geosciences, University of Edinburgh, Edinburgh, UK, [4]TNO Geological Survey of the Netherlands, Utrecht, the Netherlands

Abstract Magnetic signatures preserved in rocks have long provided insight into Earth's evolution, revealing processes from plate tectonics to the habitability of Earth. While large impacts are known to impose extreme stresses (>1 GPa) and heat that fundamentally alters magnetic records, lower stresses typical of earthquakes have been considered magnetically undetectable. We show that magnetic responses to sub-GPa stresses can be precisely calibrated, enabling three-dimensional paleostress reconstructions in rocks—even stresses of just a few MPa can fully reset magnetic signals without heat or deformation. This newly revealed magnetic sensitivity to stress opens a powerful, non-destructive pathway to detecting paleostress fields in the elastic crust, offering new opportunities for improving seismic hazard assessment, interpreting impact processes, and re-evaluating magnetic records across Earth and Planetary sciences.

Plain Language Summary Magnetic signatures preserved in rocks have long provided insights into Earth's evolution, from the birth of plate tectonic theory and helping to quantify the habitability of early Earth. Aero- and marine magnetic anomalies have revealed the scale of asteroid impacts such as Chicxulub, where high impact energies lead to stresses far in excess of 1 GPa and temperatures which melt rock. Such extreme conditions are known to strongly alter the magnetic signature of rocks; however, sub-GPa stresses, which do not cause any permanent damage such as those found near to earthquake faults and chemical explosions, have been thought too low to be magnetically recorded by rocks. Here we challenge this assumption; we show both experimentally and theoretically that stresses below 0.1 GPa measurably alter the magnetic signal of rocks without requiring heat or deformation, and that these changes can be used to fully reconstruct 3D paleo-stress vectors. This discovery of magnetic sensitivity to stress provides a novel means to detect paleostress signals within the elastic crust at radial distances away from fault cores and impact structures. This approach offers a promising tool for improving seismic hazard assessment and advancing our understanding of impact-related processes.

Key Points:

- Anisotropy of magnetic susceptibility is sensitive to pressures <1 GPa where no permanent strain occurs
- We show that the principal magnetic susceptibility vector can be used to infer the peak intensity and orientation of stress
- Numerical models support experimental observations

Supporting Information:

Supporting Information may be found in the online version of this article.

Correspondence to:

B. R. Kugabalan,
b.kugabalan22@imperial.ac.uk

Citation:

Kugabalan, B. R., Mitchell, T. M., Muxworthy, A. R., Williams, W., Gregov, H., Aben, F. M., et al. (2026). The magnetic signature of stress in rocks. *Geophysical Research Letters*, *53*, e2025GL119973. https://doi.org/10.1029/2025GL119973

Received 10 OCT 2025
Accepted 5 JAN 2026

Author Contributions:

Conceptualization: B. R. Kugabalan, T. M. Mitchell, A. R. Muxworthy, W. Williams, F. M. Aben, D. P. Dobson, P. G. Meredith
Data curation: B. R. Kugabalan, T. M. Mitchell, A. R. Muxworthy, W. Williams
Formal analysis: B. R. Kugabalan, T. M. Mitchell, A. R. Muxworthy, W. Williams, H. Gregov, U. D. Bellon
Funding acquisition: T. M. Mitchell, A. R. Muxworthy, W. Williams, U. D. Bellon, P. G. Meredith
Investigation: B. R. Kugabalan, T. M. Mitchell, A. R. Muxworthy, W. Williams
Methodology: B. R. Kugabalan, T. M. Mitchell, A. R. Muxworthy, W. Williams, H. Gregov, U. D. Bellon

1. Introduction

Stress has deformed the Earth's crust across a wide range of scales, from subtle microstructural modifications to extensive tectonic plate flexure and impact cratering (Lundstern & Zoback, 2020; Osinski et al., 2022). Accurately quantifying paleostresses is critical for understanding key geologic events such as the Chicxulub impact (Schulte et al., 2010), the evolution of the Earth and Moon (Kring et al., 2016), and the mechanics of seismic events (Brodsky et al., 2020). Traditional approaches to paleostress reconstruction—including petrographic studies of shock metamorphism and stress inversion techniques applied to fault zones (Hardebeck & Okada, 2018)—have yet to yield an accepted method for determining both the magnitude and orientation of past stresses.

These challenges highlight the need for a direct, empirical method to quantify paleostress magnitude and orientation. One promising approach is the development of rock magnetic techniques for this purpose. Magnetic signatures preserved in rocks have historically enabled major geoscientific discoveries, including the theory of plate tectonics (Vine & Matthews, 1963), but the well-documented magnetic response of rocks to stress has remained underutilized. Laboratory experiments show that mechanical stress can alter a rock's magnetization, effectively preserving a magnetic "memory" of past stress (Nagata, 1971). Building on this idea, some studies have attempted to construct a paleostress calibration curve based on explosive tests, but their method did not capture the direction of stress propagation (Martin & Noel, 1992). Rock magnetic paleostress approaches have not been developed further, largely due to two limitations: first, permanent deformation and heating at high pressures

Project administration: B. R. Kugabalan, T. M. Mitchell, A. R. Muxworthy
Resources: T. M. Mitchell, A. R. Muxworthy, W. Williams, H. Gregov
Software: W. Williams
Supervision: T. M. Mitchell, A. R. Muxworthy, W. Williams
Validation: B. R. Kugabalan, T. M. Mitchell, A. R. Muxworthy, W. Williams
Visualization: B. R. Kugabalan, T. M. Mitchell, A. R. Muxworthy, W. Williams, F. M. Aben, D. P. Dobson, P. G. Meredith
Writing – original draft: B. R. Kugabalan
Writing – review & editing: B. R. Kugabalan, T. M. Mitchell, A. R. Muxworthy, W. Williams, F. M. Aben, D. P. Dobson, U. D. Bellon, P. G. Meredith

(>1 GPa) obscure stress-induced magnetic signals (Tikoo et al., 2015); and second, it was long believed that only the smallest, uniformly magnetized single-domain (SD) particles (typically <80 nm for magnetite (Muxworthy & Williams, 2006)) could retain stable magnetic remanence over geological timescales (Bellon et al., 2025). Analytical theory further suggested that SD particles are unaffected by stresses <1 GPa (Nagata, 1971), leading to the assumption that magnetization changes in larger particles were geologically insignificant.

Recent theoretical breakthroughs overturn these assumptions, demonstrating that pseudo-single domain (PSD) particles, which exhibit vortex-state magnetization (Roberts et al., 2017), are both magnetically stable over geologic timescales and highly sensitive to stresses <1 GPa (Nagy et al., 2022; North et al., 2024). Given the ubiquity of vortex-state particles in natural rocks, this new understanding provides a foundation for a rock magnetic approach to paleostress quantification.

One promising pathway to exploit this sensitivity is through the anisotropy of magnetic susceptibility (AMS). Magnetic susceptibility characterizes the degree to which a material is reversibly magnetized in a small external field, while AMS reflects the directional dependence of this magnetization. AMS has been widely used to infer ancient flow patterns in sediments and igneous rocks (Borradaile & Jackson, 2010), because it has been interpreted to reveal the physical orientation of particles. It has long been known that magnetic susceptibility is affected by uniaxial compressive stresses (Kalashnikov & Kapitsa, 1952). However, most subsequent research has focused on AMS fabric changes associated with permanent deformation (Borradaile, 1991; Kapička, 1984), where particles have been physically rotated and displaced under stress. Since then, AMS has been used to infer fault slip directions and strain patterns in deformed regions (Elhanati et al., 2020; Ferré et al., 2015; Issachar et al., 2022). Notably, AMS has also been shown to change under stresses within the elastic limit, at pressures typically below 0.1–0.2 GPa (Kapicka, 1983; Nagata, 1970a), but this phenomenon has largely been overlooked as a potential recorder of paleostress (Ferré et al., 2025; Yang et al., 2020).

Here, we demonstrate for the first time that low-magnitude elastic stresses <150 MPa with no permanent strain, can produce significant, permanent and measurable changes in both magnetic susceptibility and AMS. Our laboratory experiments, conducted on Icelandic columnar basalts containing titanomagnetite particles with a dominant PSD population, establish a robust quantitative link between applied stress and magnetic response. Supported by state-of-the-art micromagnetic simulations, our findings reveal that even minor elastic loading can reset the magnetic fabric of rocks. This opens a direct, non-destructive pathway to reconstructing three-dimensional paleostress fields, offering a fundamentally new tool for tectonic studies, earthquake hazard assessment and planetary science.

2. Materials and Methods

For this study we chose a columnar basalt sample from Seljadalur, Iceland, from the UCL rock collection. It was chosen due to its relatively homogeneous nature (Browning et al., 2016; Vinciguerra et al., 2005). Previous studies have reported that the Seljadalur basalt consists of intergranular plagioclase, granular pyroxene, olivine and iron oxides (Browning et al., 2016), which was confirmed through optical microscopy (Figure S1 in Supporting Information S1). These basalts are rich in titanomagnetite $Fe_{2\cdot4}Ti_{0\cdot6}O_4$ (TM60; Figure S2 in Supporting Information S1), which is found in oceanic rocks making them an ideal rock type, because oceanic basalts make up ∼60% of the Earth's surface (Seton et al., 2020) and their mechanical properties are representative of other rocks (Parisio et al., 2020). The samples were found to contain magnetic particles with a log-normal mean size of 503 ± 50 nm (Figure S4 in Supporting Information S1), with strong evidence indicating predominantly magnetically determined PSD behavior (Figure S3 in Supporting Information S1). Details of all rock magnetic and grain morphology analyses are given in the Supporting Information S1.

2.1. Uniaxial Stress Experiments

To conduct differential uniaxial stress experiments a universal test frame was used at the Rock Physics Laboratory, UCL. Three types of samples were analyzed: (a) cylindrical cores 25 mm in diameter and 63 mm in length for bulk magnetic susceptibility measurements (SeljA); (b) cylindrical samples 24 mm in diameter and 20 mm in length for anisotropy of magnetic susceptibility (AMS) measurements (SeljB and SeljC); and (c) cubic samples 20 mm on a side for AMS measurements (SeljD). A cartesian coordinate system was assigned to all samples, with the z-axis along the length of the core.

The uniaxial hydraulic piston was used to compress the cylindrical samples with a strain rate of 10^{-4} s^{-1} and 10^{-3} s^{-1} for cubic samples due to the length. Both cylindrical and cubic samples were placed in between metal blocks to ensure an even distribution of stress through the samples. A linear-variable differential transformer (LVDT) was attached to the universal test frame to measure displacement and the strain of samples with accuracy better than 0.01%. We measured the force (kN) applied to the samples using the hydraulic piston and calculated the resulting peak stress (MPa).

2.2. Magnetic Susceptibility Measurements

Bulk susceptibility and the Anisotropy of Magnetic Susceptibility (AMS) of all samples were measured prior to and post uniaxial compression. Two AGICO Kappabridges were used to measure magnetic susceptibility, that is, a KLY-2 and a MFK1-FA; all the AMS measurements were made on the MFK1-FA using an automatic rotating sample holder. The susceptibility measurements were made in a 200 A/m field using a frequency of 976 Hz. AMS is characterized by three orthogonal eigenvectors: principal (maximum susceptibility) vector, $\mathbf{K_{max}}$, major (intermediate susceptibility) vector, $\mathbf{K_{int}}$, and minor (minimum susceptibility) vector, $\mathbf{K_{min}}$ (Jelínek, 1977, 1981). These eigenvectors are geometrically represented on an ellipsoid, from which the degree of anisotropy, P, and shape parameter, T, are determined (Jelínek, 1977). The shape of the ellipsoid ranges from $T = -1$ (prolate) to $T = 1$ (oblate). The mean of the susceptibility eigenvalues determines the bulk susceptibility of the samples. A standard measurement error is calculated for each eigenvector and bulk susceptibility (Jelínek, 1977). Each measurement was also subject to a positional error of order ~3°.

2.3. Numerical Micromagnetic Modeling

Micromagnetic models were simulated using the Micromagnetic Earth Related Robust Interpreted Language Laboratory (MERRILL) (Conbhuí et al., 2018) software package. We modeled particles at room temperatures with equivalent-volume spherical diameters (EVSD) of 100, 200, 300, 400, 500, 600, 700 and 800 nm with different axial ratios (AR) of 1, 1.25, 2.5 and 6. For each particle size and AR, tetrahedral finite element meshes were generated using Coreform Cubit (Coreform Cubit, 2017). Magnetic parameters such as saturation magnetization ($M_s = 1.41 \times 10^5$ A/m), exchange constant ($A_{ex} = 6.48 \times 10^{-12}$ J/m) and anisotropy constants ($K_1 = 7.72 \times 10^2$ J/m^3 and $K_2 = 2.32 \times 10^4$ J/m^3) for TM60 were supplied by MERRILL (Cych et al., 2024; Moskowitz, 1993). The mesh size was chosen to be less than the exchange length of TM60 which is ~20 nm in the unstressed state (Cych et al., 2024; Rave et al., 1998). The effect of adding stress to the model reduces the exchange length; to accommodate this we used a mesh size of 15 nm.

The starting point for all simulations was the absolute energy minimum domain state (AEM) determined from 50 random initial guess solutions. The pre-stress susceptibility of the particles was determined in 50 field directions (selected from a Fibonacci distribution to obtain a near-uniform distribution), in a simulated DC magnetic field of 0.25 mT. To simulate a randomly orientated distribution 50 orientations were also selected from a Fibonacci distribution; that is, for each particle 2,500 combinations of relative particle and field orientations were considered. Subsequently, a uniaxial stress of 20 MPa (Figure 3) and 150 MPa (Figure S5 in Supporting Information S1) was modeled. This was chosen based on the experimental data measured as part of this study and from reported data (Sahu & Moskowitz, 1995). This results in an additional anisotropy energy term (E_σ) within MERRILL which accounts for magnetoelastic energy:

$$E_\sigma = \frac{3}{2}\sigma\lambda_{001} V \sin 2\theta \quad (1)$$

where σ is the stress in the [0,0,1] direction, λ_{001} is the magnetostriction constant in this direction (for TM60 at room temperature $\lambda_{001} = 142.5 \times 10^{-6}$; Sahu & Moskowitz, 1995), V is the volume, θ is the angle between the magnetization and applied stress axis. After the uniaxial stress was released the susceptibility of the particles "post-stressed" state was calculated to examine the change in susceptibility. The overall changes in susceptibility between the non-stressed and post-stressed states were calculated for each particle size and AR using least squares fitting after data regularization. Regularization averaged the data over 50 uniform azimuthal sectors of a sphere, which helped to reduce noise before performing least square fit to an ellipsoid surface. From the ellipsoid fittings three eigenvectors were determined which indicated the changes in the principal susceptibility vector. The

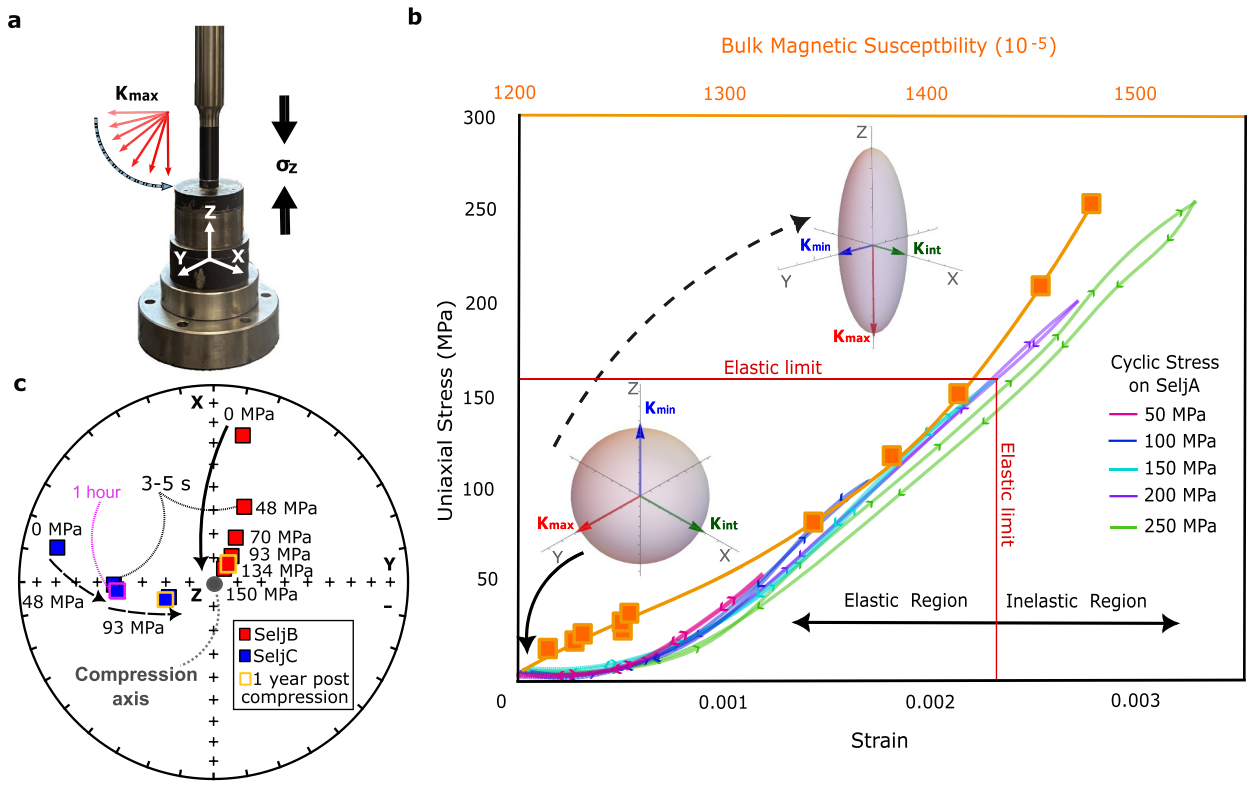

Figure 1. Rock mechanical and magnetic effects on cylindrical samples under uniaxial stress. (a) A cylindrical sample placed under uniaxial hydraulic compression and stress, σ_z, applied vertically in the *z*-axis of the system. Initially $\mathbf{K_{max}}$ was aligned close to the *x*-*y* plane with increasing compression $\mathbf{K_{max}}$ aligned with the *z*-axis. (b) Cyclic stress-strain measurements indicate an elastic limit of ∼160 MPa for our samples. The orange curve is the increase in magnetic susceptibility measured after the application of stress on sample SeljA. The change in the AMS ellipsoid's shape, *T*, is illustrated schematically: as the stress increases, *T* changes from being near isotropic prior to compression to a prolate ellipsoid with the $\mathbf{K_{max}}$ aligned with the compression *z*-axis. (c) An equal area projection showing the orientation of $\mathbf{K_{max}}$ in response to increasing σ_z with ±1° error uncertainty. SeljB was subjected to peak stresses for ∼3–5 s. SeljC was held under uniaxial compression at 48 MPa initially for ∼3–5 s and then for 1 hr, the stress was then approximately doubled to 93 MPa. In both cases the strain rate during loading was 10^{-4} s^{-1}. Repeat measurements made a year after the experiments are highlighted in yellow.

absolute value of the degree of anisotropy, *P*-1, was determined for all particle sizes and ARs. By definition, *P*-1 = 0 for spheres, while *P*-1 > 0 indicates measurable anisotropy.

3. Results

3.1. Experimental

Icelandic columnar basalts were used to perform quasi-static uniaxial stress tests (Figure 1a). Under compression, 23 ± 1% increase in magnetic susceptibility is observed up to 250 MPa in sample SeljA (Figure 1b). Prior to compression, the AMS ellipsoid was near spherical ($T \sim 0$) with weak anisotropy ($P \sim 1$; V. Jelínek, 1981), which means that the susceptibility was near isotropic (Figure 1b). Under the application of cyclic uniaxial stress, the susceptibility increased in magnitude (Figure 1b) and became increasingly prolate with $P > 1$, with $\mathbf{K_{max}}$, gradually aligning with the compression axis (Figure 1b). This increase in susceptibility magnitude was consistent up to 250 MPa, which is beyond the elastic limit of SeljA, which became inelastic at ∼160 MPa (Figure 1b). The $\mathbf{K_{max}}$ vector rotates toward the compression axis with increasing stress. This behavior was observed for two sister samples (SeljB and SeljC), which both had their initial $\mathbf{K_{max}}$ vectors aligned almost perpendicular to the compression axis (Figure 1c). We performed two compression routines for these two samples. SeljB was subjected to cyclic loading with increasing peak stress, with each stress cycle held at peak stress for ∼3–5 s. The maximum applied stress for this sample was 150 MPa, within the elastic regime (Figure 1c). In contrast, SeljC was initially held under 48 MPa for ∼3–5 s followed by an AMS measurement. This was subsequently repeated holding the sample under 48 MPa for 1 hr. There was no significant change in the rotation in $\mathbf{K_{max}}$ (32 ± 1°) after the second repeat experiment (<1%). We then approximately doubled the peak stress to 93 MPa (holding time 3–5 s), and $\mathbf{K_{max}}$

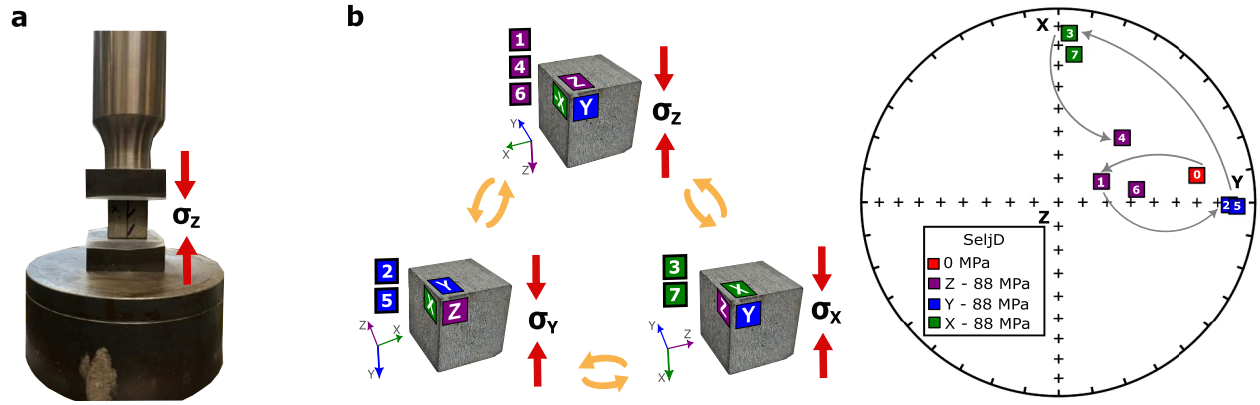

Figure 2. $\mathbf{K_{max}}$ response from uniaxial loading on a cyclically rotated cube. (a) A schematic of the cube experiment set up under the uniaxial hydraulic compressor. (b) A cubic sample (SeljD) was compressed at 88 MPa using a loading strain rate of 10^{-3} s^{-1}. The stress was applied cyclically in all three axes *x, y* and *z*. $\mathbf{K_{max}}$ was initially in the *x*-*y* plane (position 0, 0 MPa) and rotated toward the *z*-axis under compression in *z* (position 1). Subsequent AMS measurements (positions 2, 3, 4 etc.) followed compressions in *x, y* and *z*. Permanent deformation began to occur after position 4.

rotated toward the compression axis. After 93 MPa SeljB and SeljC have similar $\mathbf{K_{max}}$ inclinations, that is, 77 ± 1° and 73 ± 1° respectively. This critical finding suggests that $\mathbf{K_{max}}$ rotation depends solely on the peak stress experienced, not the exposure time (Figure 1c). A linear behavior is observed up to a saturation threshold beyond which $\mathbf{K_{max}}$ becomes fully aligned with the stress axis and remains unchanged with increasing stress. This saturation behavior indicates that AMS records the maximum experienced stress, rather than accumulating overprints from successive lower stresses. For both samples, the AMS measurements were repeated 1 year after the stress experiments, with the samples having been kept at room-temperature in an ambient field. There was found to be <1% change in the $\mathbf{K_{max}}$, $\mathbf{K_{int}}$ and $\mathbf{K_{min}}$ direction (Figure 1c).

To determine the reversibility of this AMS response to applied stress and direction, we cyclically loaded a cubic sample (SeljD) along different axes *x, y* and *z* at a strain rate of 10^{-3} s^{-1} (Figure 2a). Again, the pre-compression state of the $\mathbf{K_{max}}$ vector was initially in the *x*-*y* plane (Figure 2b). We compressed the sample using a stress of 88 MPa in the *z*-axis, followed by subsequent compressions in all three axes always using a peak stress of 88 MPa (Figure 2b). After each compression, the $\mathbf{K_{max}}$ vector rotated close to the last applied compression direction (Figure 2b). Beyond the fourth compression step in the *z*-direction, fractures began to visibly appear in the sample, thus becoming inelastic and $\mathbf{K_{max}}$ did not align as closely with the applied stress direction as seen in earlier steps.

3.2. Micromagnetic Models

In the numerical models the pre-stressed state was entirely symmetric, that is, the AMS was isotropic. After simulating a 20 MPa (Figure 3) and 150 MPa (Figure S5 in Supporting Information S1) uniaxial stress along the *z*-axis and subsequently releasing the stress and numerically estimating the AMS of the models, we found that the response of the SD and vortex-state particles is diametrically opposite (Figure 3). Under stress, the magnetization of the SD particles aligns perpendicular to the stress direction, that is, in the compression plane, as predicted by analytical theory (Nagata, 1970b). On release of the stress the SD particles partially relax out of the compression plane. When the AMS is calculated, it is maximal along the compression axis, because it is easier for the magnetization to rotate out of the compression plane, where it is already aligned, than back into it. The effect of this is to align the $\mathbf{K_{max}}$ vector with the compression axis. The response of vortex-state particles is the opposite. In our models, these displayed single-vortex (SV) structures, where magnetization curls around a central core (Williams & Dunlop, 1989). In SV particles it is generally the vortex core that carries the magnetization remanence, with the curling outer-particle magnetization contributing little to the net magnetic vector. After applying the stress within the model, the core of SV particles aligns with compression axis, because the energy of the magnetic structure is minimized by rotating the outer-curling magnetic vector into the compression plane. On determining the AMS, it is now easier for the magnetization to rotate away from the compression axis into the plane, making $\mathbf{K_{max}}$ aligned in the compression plane, and $\mathbf{K_{min}}$ aligned with the compression axis. For a distribution of randomly orientated particles, the contribution to the resultant $\mathbf{K_{max}}$ from SD particles is to enhance $\mathbf{K_{max}}$ in the compression axis, and the net effect of vortex-state assemblies is to contribute to $\mathbf{K_{max}}$ in the

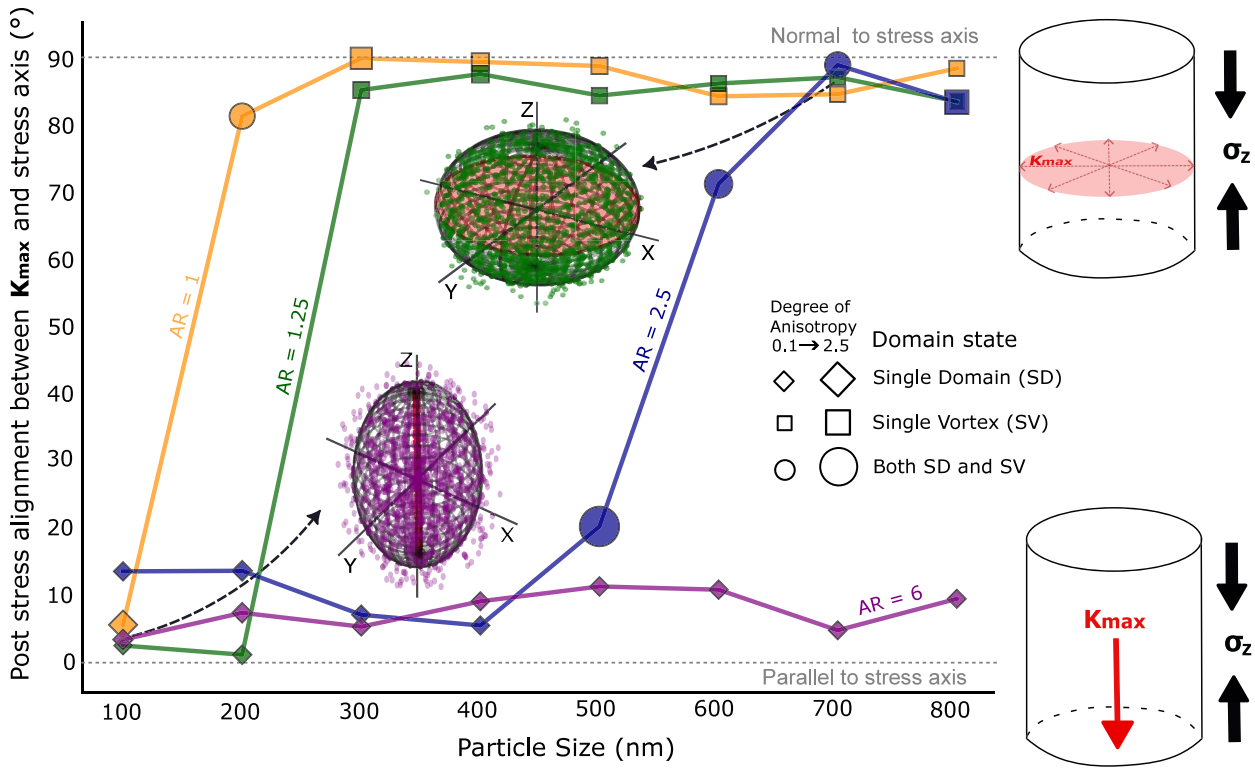

Figure 3. Micromagnetic model results illustrating the alignment of **Kmax** of a random distribution of SD and vortex-state particles after simulating the application and removal of a 20 MPa of uniaxial stress in the z-axis, that is, post stress. The alignment of the $\mathbf{K}_{max}$ vector relative to the stress axis, following the application of 20 MPa uniaxial stress, is shown as a function of axial ratio (AR) and particle size (EVSD). The domain state of the particles at different EVSD and AR are highlighted using different shaped points and the size of the points reflect the AMS degree of anisotropy, *P*-1. The AMS shapes after 20 MPa stress are illustrated: SD particles (100 nm, AR = 6) give rise to a prolate AMS ellipsoid with $\mathbf{K}_{max}$ parallel to the compression axis. As particle size increases—where particles exhibit SV states (700 nm, AR = 1.25)—the AMS ellipsoid becomes oblate, with $\mathbf{K}_{max}$ oriented parallel to the compression plane.

compression plane. However, as the $\mathbf{K}_{max}$ contribution from an SV particle can be aligned to the nearest easy axis direction in the compression plane, the resultant $\mathbf{K}_{max}$ from a random assemblage of vortex-state particles is zero. This is seen in Figure 3, where the smaller 100 nm particles, which are all SD, have $\mathbf{K}_{max}$ aligned with the compression axis. As particle size increases in the model, a larger proportion of particles transition to SV states, with the exact threshold size strongly dependent on AR (Cych et al., 2024). As the particle size transitions from SD to vortex behavior, $\mathbf{K}_{max}$ rotates from alignment with the compression axis to alignment with the compression plane. For the extreme case very elongated particles, in our models where AR = 6 (a needle shape), the magnetization is SD even at 800 nm and the $\mathbf{K}_{max}$ is aligned with the compression axis (Figure 3).

We also calculated the absolute value of the degree of anisotropy, *P*-1, for our modeled data, which is reflected in the size of the marker points (Figure 3). For highly prolate particles, like AR = 6, the applied stress has virtually no effect on its domain state. In that case the AMS ellipsoid is nearly spherical, and the *P*-1 values remain close to zero. When stress has a significant effect on domain state, then the AMS becomes anisotropic, for example, for particles with AR <2.5, and this reflected in larger values of *P* (Figure 3).

4. Discussion

Overall, our experimental and numerical results demonstrate that both the direction and, with calibration, the magnitude of peak elastic stresses (<160 MPa) can be reconstructed from AMS measurements (Figures 1–3). Our Icelandic basalt samples, with a log-normal meanTM60 particle size of 503 nm and axial ratio of 1.76, display stress-induced AMS signatures consistent with SD-dominated behavior (Figure 4), despite lying predominantly in the vortex-stability region (Cych et al., 2024). Our theoretical framework shows that in mixed SD and vortex-state particle populations, vortex-state particles may obscure the stress signal, potentially yielding more isotropic or oblate fabrics (Figure 3). Single-domain (SD) particles contribute to $\mathbf{K}_{max}$ alignment along the compression axis;

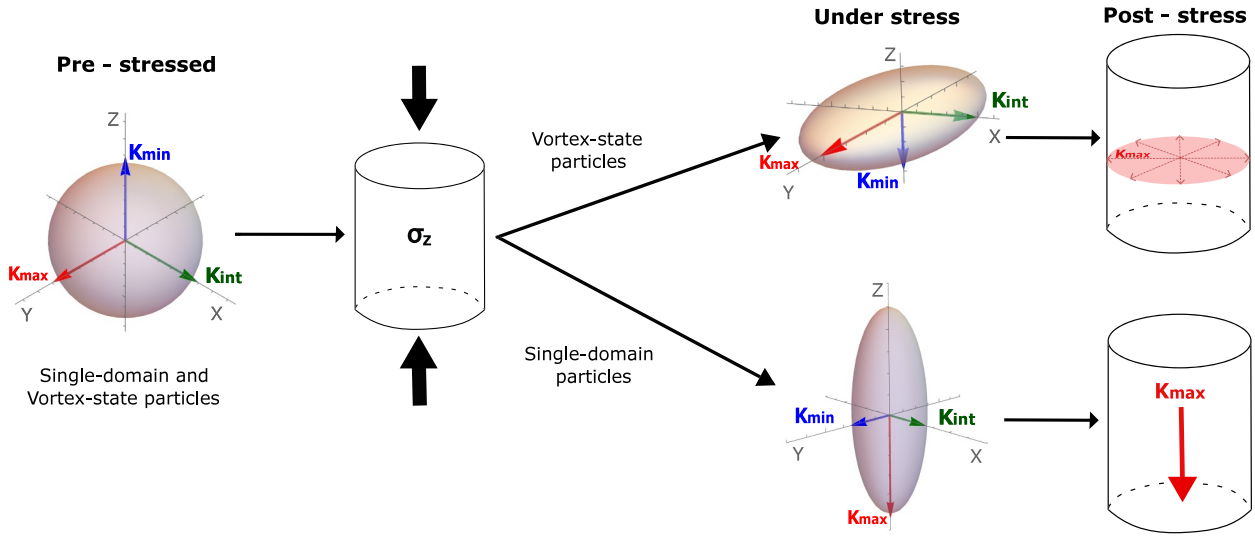

Figure 4. Overall schematic summarizing the simulated and experimental results. The initial pre-stress AMS shape resulting from the random distribution of single-domain (SD) and vortex-state particles are isotropic, as observed in our experimental samples. Under uniaxial stress, the AMS vectors rotate and increase in magnitude, with the shape becoming oblate for vortex-state particles and prolate for SD particles. After stress application $\mathbf{K_{max}}$ shows two distinct orientations: vortex-state particles align normal to the compression plane, while SD particles align parallel to the compression axis, both effectively recording the stress signal.

however, vortex-state particles contribute negligibly to the net AMS fabric (Figure 4). The elastically stress-induced AMS signals appear to be geologically stable over extended timescales, as evidenced by the reproducibility of AMS measurements 1 year after initial compression (Figure 1c) and consistent with theoretical expectations for SD and vortex-state particles (Nagy et al., 2017).

4.1. AMS as Hidden Records of Stress

To quantify paleostress from natural rocks, it will be necessary to combine AMS measurements with lithology-specific mechanical calibration curves (Yang et al., 2020). Different rock types and magnetic mineral assemblages respond variably to differential stress, depending on their mechanical strength, particle size distribution, and magnetic domain state (Bhowmick et al., 2025; Elhanati et al., 2021; Weinberger et al., 2022); in contrast to their behavior under hydrostatic conditions (Figure S6 in Supporting Information S1).

Our study indicates that $\mathbf{K_{max}}$ records the maximum peak stress experienced during an event. Lower-magnitude stresses, that is, aftershocks, are unlikely to overwrite the dominant signal in the country rock. Stress fields decay with distance from the fault core approximately as $1/r^{3/2}$ and similar relation for impact craters (Collins et al., 2004; Doan & Gary, 2009), meaning that sampling at strategic radial distances allows separation of elastic stress signatures from deformation, hydrothermal or thermal overprints (Tikoo et al., 2015; Ujiie et al., 2003). Although AMS signals also persist within the inelastic deformation zone, they are difficult to disentangle from the stress signal because of physical grain rotations, particle displacements and cracking, with the overall response dominated by alteration (Ferré et al., 2025). Brittle fracture zones are typically confined within hundreds of meters of faults, elastic stress fields propagate much farther into the surrounding country rock (Aben et al., 2020), offering the potential to resolve multiple seismic events from a fault as well as from adjacent craters. Determining the asymmetric paleostress fields in the country rock enables us to retrace the shock propagation from the focal mechanism or point of impact. Where present, pseudotachylytes formed during seismic slip and impact events from frictional heating (Ferré et al., 2015; Melosh, 2005) can constrain event timing, anchoring AMS-based paleostress analyses in geologic time.

5. Conclusions

Our study reveals that magnetic fabrics in rocks can act as sensitive, durable recorders of paleostress. We show that elastic stresses with no permanent strain can leave stable, recoverable and exclusively magnetic imprints in rocks, revealing a previously hidden recorder of ancient stress fields. Although further validation across broader

lithologic and structural settings, as well as varied differential stress regimes, is needed, the results presented here provide a critical steppingstone toward using magnetic fabrics to reconstruct earthquake, impact and tectonic processes at unprecedented scales. Ultimately, the methods described here have the potential to constrain key earthquake source parameters, including rupture directivity and fault scaling relationships, with major implications for seismic hazard assessment, planetary geology and resource exploration.

Conflict of Interest

The authors declare no conflicts of interest relevant to this study.

Data Availability Statement

All raw data related to this manuscript and supporting information are archived on Zenodo and is publicly accessible (see https://doi.org/10.5281/ZENODO.17294343 in Kugabalan et al. (2025)).

Acknowledgments

We gratefully acknowledge P.G.M and Prof Stan Murrell from UCL for collecting the Seljadalur columnar basalts in Iceland with help from Prof. Agust Gudmundsson (Royal Holloway) who was at the time at University of Iceland. The fieldtrip to Iceland was funded by NERC during the 1990s, which was awarded to P.G.M and Prof. Stan Murrell. B.K acknowledges the Janet Watson PhD scholarship, ESE, Imperial College London. T.M.M, A.R.M, W.W and U.D.B would like to acknowledge support from the Natural Environment Research Council (NERC) through Grants NE/Z000068/1, NE/W006707/1, NE/V001388/1 and NE/M004716/1. A.R.M would also like to acknowledge support from the UK Research and Innovation (UKRI), Engineering and Physical Sciences Research Council (EPSRC) Grant EP/X02878X/1.

References

Aben, F. M., Doan, M.-L., & Mitchell, T. M. (2020). Variation of hydraulic properties due to dynamic fracture damage: Implications for fault zones. *Journal of Geophysical Research: Solid Earth*, *125*(4), e2019JB018919. https://doi.org/10.1029/2019JB018919

Bellon, U. D., Williams, W., Muxworthy, A. R., Souza-Junior, G. F., Nagy, L., Uieda, L., & Trindade, R. I. F. (2025). Efficiency of thermoremanent magnetization acquisition in vortex-state particle assemblies. *Geophysical Research Letters*, *52*(8), e2025GL114771. https://doi.org/10.1029/2025GL114771

Bhowmick, S., Levi, T., Boneh, Y., Marco, S., Yang, T., Meher, B., & Weinberger, R. (2025). Magnetic and microstructural perspectives on faulting in carbonate rocks, Northern Israel. *Journal of Structural Geology*, *198*, 105436. https://doi.org/10.1016/j.jsg.2025.105436

Borradaile, G. J. (1991). Correlation of strain with anisotropy of magnetic susceptibility (AMS). *Pure and Applied Geophysics*, *135*(1), 15–29. https://doi.org/10.1007/BF00877006

Borradaile, G. J., & Jackson, M. (2010). Structural geology, petrofabrics and magnetic fabrics (AMS, AARM, AIRM). *Journal of Structural Geology*, *32*(10), 1519–1551. https://doi.org/10.1016/j.jsg.2009.09.006

Brodsky, E. E., Mori, J. J., Anderson, L., Chester, F. M., Conin, M., Dunham, E. M., et al. (2020). The state of stress on the fault before, during, and after a major earthquake. *Annual Review of Earth and Planetary Sciences*, *48*(1), 49–74. https://doi.org/10.1146/annurev-earth-053018-060507

Browning, J., Meredith, P., & Gudmundsson, A. (2016). Cooling-dominated cracking in thermally stressed volcanic rocks. *Geophysical Research Letters*, *43*(16), 8417–8425. https://doi.org/10.1002/2016GL070532

Collins, G. S., Melosh, H. J., & Ivanov, B. A. (2004). Modeling damage and deformation in impact simulations. *Meteoritics & Planetary Sciences*, *39*(2), 217–231. https://doi.org/10.1111/j.1945-5100.2004.tb00337.x

Conbhuí, P. Ó., Williams, W., Fabian, K., Ridley, P., Nagy, L., & Muxworthy, A. R. (2018). MERRILL: Micromagnetic earth related robust interpreted language laboratory. *Geochemistry, Geophysics, Geosystems*, *19*(4), 1080–1106. https://doi.org/10.1002/2017GC007279

Coreform Cubit. (2017). (Version 16.4). Coreform LLC. Retrieved from https://coreform.com

Cych, B., Paterson, G. A., Nagy, L., Williams, W., & Moskowitz, B. (2024). Magnetic domain states and critical sizes in the titanomagnetite series. *Journal of Geophysical Research: Solid Earth*, *129*(6), e2024JB028805. https://doi.org/10.1029/2024JB028805

Doan, M.-L., & Gary, G. (2009). Rock pulverization at high strain rate near the San Andreas fault. *Nature Geoscience*, *2*(10), 709–712. https://doi.org/10.1038/ngeo640

Elhanati, D., Issachar, R., Levi, T., & Weinberger, R. (2021). A practical approach for identification of magnetic fabric carriers in rocks. *Journal of Geophysical Research: Solid Earth*, *126*(5), e2020JB021105. https://doi.org/10.1029/2020jb021105

Elhanati, D., Levi, T., Marco, S., & Weinberger, R. (2020). Zones of inelastic deformation around surface ruptures detected by magnetic fabrics. *Tectonophysics*, *788*, 228502. https://doi.org/10.1016/j.tecto.2020.228502

Ferré, E. C., Geissman, J. W., Chauvet, A., Vauchez, A., & Zechmeister, M. S. (2015). Focal mechanism of prehistoric earthquakes deduced from pseudotachylyte fabric. *Geology*, *43*(6), 531–534. https://doi.org/10.1130/G36587.1

Ferré, E. C., Li, H., Zamani, N., Milesi, G., & Li, J. (2025). Thermochronological and magnetic advances on faulting processes: An introduction. *Journal of Structural Geology*, 105491. https://doi.org/10.1016/j.jsg.2025.105491

Hardebeck, J. L., & Okada, T. (2018). Temporal stress changes caused by Earthquakes: A review. *Journal of Geophysical Research: Solid Earth*, *123*(2), 1350–1365. https://doi.org/10.1002/2017JB014617

Issachar, R., Levi, T., & Weinberger, R. (2022). Differentiating between remote and local strain fields near mesoscale faults by magnetic fabrics in deformed chalks. *Journal of Structural Geology*, *155*, 104524. https://doi.org/10.1016/j.jsg.2022.104524

Jelínek, V. (1977). The statistical theory of measuring anisotropy of magnetic susceptibility of rocks and its application.

Jelínek, V. (1981). Characterization of the magnetic fabric of rocks. *Tectonophysics*, *79*(3–4), T63–T67. https://doi.org/10.1016/0040-1951(81)90110-4

Kalashnikov, A., & Kapitsa, S. (1952). Magnetic susceptibility of elastically stressed rocks. *Proc.(Doclady) Acad. Sci. USSR*, *86*, 521–523.

Kapicka, A. (1983). Irreversible changes of anisotropy of magnetic susceptibility of rocks due to uniaxial pressure. *Journal of Geophysics - Zeitschrift Fur Geophysik*, *53*(3), 144–148.

Kapička, A. (1984). Magnetic susceptibility anisotropy of deformed rocks. *Studia Geophysica et Geodaetica*, *28*(1), 90–100. https://doi.org/10.1007/BF01587113

Kring, D. A., Kramer, G. Y., Collins, G. S., Potter, R. W. K., & Chandnani, M. (2016). Peak-ring structure and kinematics from a multi-disciplinary study of the Schrödinger impact basin. *Nature Communications*, *7*(1), 13161. https://doi.org/10.1038/ncomms13161

Kugabalan, B., Mitchell, T., Muxworthy, A., Williams, W., Gergov, H., Aben, F., et al. (2025). The paleomagnetic signature of stress in rocks [Dataset]. *Zenodo*. https://doi.org/10.5281/ZENODO.17294343

Lundstern, J.-E., & Zoback, M. D. (2020). Multiscale variations of the crustal stress field throughout North America. *Nature Communications*, *11*(1), 1951. https://doi.org/10.1038/s41467-020-15841-5

Martin, R. J., & Noel, J. S. (1992). Dynamic stress measurements using piezomagnetism (p. ARMA-92-0069). Presented at the The 33rd U.S. Symposium on Rock Mechanics (USRMS).
Melosh, H. J. (2005). The mechanics of pseudotachylite formation in impact events. In C. Koeberl & H. Henkel (Eds.), *Impact tectonics* (pp. 55–80). Springer Berlin Heidelberg. https://doi.org/10.1007/3-540-27548-7_2
Moskowitz, B. M. (1993). High-temperature magnetostriction of magnetite and titanomagnetites. *Journal of Geophysical Research*, *98*(B1), 359–371. https://doi.org/10.1029/92JB01846
Muxworthy, A. R., & Williams, W. (2006). Critical single-domain/multidomain grain sizes in noninteracting and interacting elongated magnetite particles: Implications for magnetosomes. *Journal of Geophysical Research*, *111*(B12). https://doi.org/10.1029/2006JB004588
Nagata, T. (1970a). Anisotropic magnetic susceptibility of rocks under mechanical stresses. *Pure and Applied Geophysics*, *78*(1), 110–122. https://doi.org/10.1007/BF00874779
Nagata, T. (1970b). Basic magnetic properties of rocks under the effects of mechanical stresses. *Tectonophysics*, *9*(2), 167–195. https://doi.org/10.1016/0040-1951(70)90015-6
Nagata, T. (1971). Introductory notes on shock remanent magnetization and shock demagnetization of igneous rocks. *Pure and Applied Geophysics*, *89*(1), 159–177. https://doi.org/10.1007/BF00875213
Nagy, L., Williams, W., Muxworthy, A. R., Fabian, K., Almeida, T. P., Conbhuí, P. Ó., & Shcherbakov, V. P. (2017). Stability of equidimensional pseudo–single-domain magnetite over billion-year timescales. *Proceedings of the National Academy of Sciences*, *114*(39), 10356–10360. https://doi.org/10.1073/pnas.1708344114
Nagy, L., Williams, W., Tauxe, L., & Muxworthy, A. (2022). Chasing tails: Insights from micromagnetic modeling for thermomagnetic recording in non-uniform magnetic structures. *Geophysical Research Letters*, *49*(23), e2022GL101032. https://doi.org/10.1029/2022GL101032
North, T. L., Muxworthy, A. R., Williams, W., Mitchell, T. M., Collins, G. S., & Davison, T. M. (2024). The effect of stress on paleomagnetic signals: A micromagnetic study of magnetite's single-vortex response. *Geophysical Research Letters*, *51*(2), e2023GL106868. https://doi.org/10.1029/2023GL106868
Osinski, G. R., Grieve, R. A. F., Ferrière, L., Losiak, A., Pickersgill, A. E., Cavosie, A. J., et al. (2022). Impact Earth: A review of the terrestrial impact record. *Earth-Science Reviews*, *232*, 104112. https://doi.org/10.1016/j.earscirev.2022.104112
Parisio, F., Lehmann, C., & Nagel, T. (2020). A model of failure and localization of basalt at temperature and pressure conditions spanning the brittle-ductile transition. *Journal of Geophysical Research: Solid Earth*, *125*(11), e2020JB020539. https://doi.org/10.1029/2020JB020539
Rave, W., Fabian, K., & Hubert, A. (1998). Magnetic states of small cubic particles with uniaxial anisotropy. *Journal of Magnetism and Magnetic Materials*, *190*(3), 332–348. https://doi.org/10.1016/s0304-8853(98)00328-x
Roberts, A. P., Almeida, T. P., Church, N. S., Harrison, R. J., Heslop, D., Li, Y., et al. (2017). Resolving the origin of pseudo-single domain magnetic behavior. *Journal of Geophysical Research: Solid Earth*, *122*(12), 9534–9558. https://doi.org/10.1002/2017JB014860
Sahu, S., & Moskowitz, B. M. (1995). Thermal dependence of magnetocrystalline anisotropy and magnetostriction constants of single crystal Fe2,4Ti0.61O4. *Geophysical Research Letters*, *22*(4), 449–452. https://doi.org/10.1029/94GL03296
Schulte, P., Alegret, L., Arenillas, I., Arz, J. A., Barton, P. J., Bown, P. R., et al. (2010). The Chicxulub asteroid impact and mass extinction at the Cretaceous-Paleogene boundary. *Science*, *327*(5970), 1214–1218. https://doi.org/10.1126/science.1177265
Seton, M., Müller, R. D., Zahirovic, S., Williams, S., Wright, N. M., Cannon, J., et al. (2020). A global data set of present-day oceanic crustal age and seafloor spreading parameters. *Geochemistry, Geophysics, Geosystems*, *21*(10), e2020GC009214. https://doi.org/10.1029/2020GC009214
Tikoo, S. M., Gattacceca, J., Swanson-Hysell, N. L., Weiss, B. P., Suavet, C., & Cournède, C. (2015). Preservation and detectability of shock-induced magnetization. *Journal of Geophysical Research: Planets*, *120*(9), 1461–1475. https://doi.org/10.1002/2015JE004840
Ujiie, K., Hisamitsu, T., & Taira, A. (2003). Deformation and fluid pressure variation during initiation and evolution of the plate boundary décollement zone in the Nankai accretionary prism. *Journal of Geophysical Research*, *108*(B8). https://doi.org/10.1029/2002JB002314
Vinciguerra, S., Trovato, C., Meredith, P. G., & Benson, P. M. (2005). Relating seismic velocities, thermal cracking and permeability in Mt. Etna and Iceland basalts. *Rock Physics and Geomechanics*, *42*(7), 900–910. https://doi.org/10.1016/j.ijrmms.2005.05.022
Vine, F. J., & Matthews, D. H. (1963). Magnetic anomalies over oceanic ridges. *Nature*, *199*(4897), 947–949. https://doi.org/10.1038/199947a0
Weinberger, R., Alsop, G. I., & Levi, T. (2022). Magnetic fabrics as strain markers in folded soft-sediment layers. *Journal of Structural Geology*, *155*, 104513. https://doi.org/10.1016/j.jsg.2022.104513
Williams, W., & Dunlop, D. J. (1989). Three-dimensional micromagnetic modelling of ferromagnetic domain structure. *Nature*, *337*(6208), 634–637. https://doi.org/10.1038/337634a0
Yang, T., Chou, Y.-M., Ferré, E. C., Dekkers, M. J., Chen, J., Yeh, E.-C., & Tanikawa, W. (2020). Faulting processes unveiled by magnetic properties of fault rocks. *Reviews of Geophysics*, *58*(4), e2019RG000690. https://doi.org/10.1029/2019RG000690

References From the Supporting Information

Akimoto, S., Katsura, T., & Yoshida, M. (1957). Magnetic properties of $TiFe_2O_4$-Fe_3O_4 system and their change with oxidation. *Journal of Geomagnetism and Geoelectricity*, *9*(4), 165–178. https://doi.org/10.5636/jgg.9.165
Browning, J., Meredith, P., & Gudmundsson, A. (2016). Cooling-dominated cracking in thermally stressed volcanic rocks. *Geophysical Research Letters*, *43*(16), 8417–8425. https://doi.org/10.1002/2016GL070532
Cych, B., Paterson, G. A., Nagy, L., Williams, W., & Moskowitz, B. (2024). Magnetic domain states and critical sizes in the titanomagnetite series. *Journal of Geophysical Research: Solid Earth*, *129*(6), e2024JB028805. https://doi.org/10.1029/2024JB028805
Kapicka, A. (1983). Irreversible changes of anisotropy of magnetic susceptibility of rocks due to uniaxial pressure. *Journal of Geophysics - Zeitschrift Fur Geophysik*, *53*(3), 144–148.
Muxworthy, A. R., & Williams, W. (2005). Magnetostatic interaction fields in first-order-reversal-curve diagrams. *Journal of Applied Physics*, *97*(6), 063905. https://doi.org/10.1063/1.1861518
Muxworthy, A. R., & Dunlop, D. J. (2002). First-order reversal curve (FORC) diagrams for pseudo-single-domain magnetites at high temperature. *Earth and Planetary Science Letters*, *203*(1), 369–382. https://doi.org/10.1016/S0012-821X(02)00880-4
Nagy, L., Williams, W., Tauxe, L., & Muxworthy, A. R. (2019). From nano to micro: Evolution of magnetic domain structures in multidomain magnetite. *Geochemistry, Geophysics, Geosystems*, *20*(6), 2907 2918–2918. https://doi.org/10.1029/2019GC008319
Nagy, L., Moreno, R., Muxworthy, A. R., Williams, W., Paterson, G. A., Tauxe, L., & Valdez-Grijalva, M. A. (2024). Micromagnetic determination of the FORC response of paleomagnetically significant magnetite assemblages. *Geochemistry, Geophysics, Geosystems*, *25*(7), e2024GC011465. https://doi.org/10.1029/2024GC011465

Nulman, A. A., Shapiro, V. A., Maksimovskikh, S. I., Ivanov, N. A., Kim, J., & Carmichael, R. S. (1978). Magnetic susceptibility of magnetite under hydrostatic pressure, and implications for tectonomagnetism. *Journal of Geomagnetism and Geoelectricity*, *30*(5), 585–592. https://doi.org/10.5636/jgg.30.585

Roberts, A. P., Pike, C. R., & Verosub, K. L. (2000). First-order reversal curve diagrams: A new tool for characterizing the magnetic properties of natural samples. *Journal of Geophysical Research: Solid Earth*, *105*(B12), 28461–28475. https://doi.org/10.1029/2000JB900326

Roberts, A. P., Heslop, D., Zhao, X., & Pike, C. R. (2014). Understanding fine magnetic particle systems through use of first-order reversal curve diagrams. *Reviews of Geophysics*, *52*(4), 557–602. https://doi.org/10.1002/2014RG000462